Single-, double-, and triple-slit diffraction of molecular matter waves

Christian Brand, Stephan Troyer, Christian Knobloch, et al.

Citation: American Journal of Physics **89**, 1132 (2021); doi: 10.1119/5.0058805
View online: https://doi.org/10.1119/5.0058805
View Table of Contents: https://aapt.scitation.org/toc/ajp/89/12
Published by the American Association of Physics Teachers

Single-, double-, and triple-slit diffraction of molecular matter waves

Christian Brand[a)]
Faculty of Physics, University of Vienna, Boltzmanngasse 5, A-1090 Vienna, Austria and German Aerospace Center (DLR), Institute of Quantum Technologies, Söflinger Straße 100, 89077 Ulm, Germany

Stephan Troyer
Faculty of Physics, University of Vienna, Boltzmanngasse 5, A-1090 Vienna, Austria

Christian Knobloch
Faculty of Physics, University of Vienna, Boltzmanngasse 5, A-1090 Vienna, Austria

Ori Cheshnovsky
Tel Aviv University, The Center for Nanosciences and Nanotechnology, Tel Aviv 69978, Israel and School of Chemistry, The Raymond and Beverly Faculty of Exact Sciences, Tel Aviv University, Tel Aviv 69978, Israel

Markus Arndt
Faculty of Physics, University of Vienna, Boltzmanngasse 5, A-1090 Vienna, Austria

(Received 2 June 2021; accepted 13 August 2021)

Even 100 years after its introduction by Louis de Broglie, the wave-nature of matter is often regarded as a mind-boggling phenomenon. To give an intuitive introduction to this field, we here discuss the diffraction of massive molecules through a single, a double, and a triple slit, as well as a nanomechanical grating. While the experiments are in good agreement with undergraduate textbook predictions, we also observe pronounced differences resulting from the molecules' mass and internal complexity. The molecules' polarizability causes an attractive van der Waals interaction with the slit walls, which can be modified by rotating the nanomechanical mask with respect to the molecular beam. The text is meant to introduce students and teachers to the concepts of molecule diffraction, supported by problems and solutions that can be discussed in class.
https://doi.org/10.1119/5.0058805

I. INTRODUCTION

Due to its conceptual simplicity, diffraction at single and double slits is often used to illustrate the principles of wave optics. Extending this idea to matter waves then serves to illustrate the wave-particle duality and the superposition principle for massive particles in quantum mechanics. The present work summarizes the analogies and differences of light and particle optics in the context of recent molecule diffraction experiments. We show that a proper description needs to include internal particle properties such as the polarizability, even though the de Broglie wavelength contains only information about the center of mass motion.

Matter-wave diffraction through a few slits ($N = 1 - 3$) has been demonstrated for electrons,[1–3] neutrons,[4,5] atoms,[6–9] and molecules,[10,11] using mostly micro- or nanopatterned membranes. The possibility to realize even complex structures with nanometer precision in these materials led to the fabrication of slits[6] and gratings,[12] sieves,[13,14] and holograms.[15] They are used to focus beams of neutral helium[16] and study weakly bound clusters[17,18] as well as higher-order matter-wave interference.[11,19] Nanomechanical gratings became essential for three-grating interferometers with electrons,[20,21] neutrons,[22] atoms,[23] and molecules[24–26] up to masses beyond 25 000 u—and even for experiments with antimatter.[27]

Here, we put molecule diffraction at nanomechanical masks into a pedagogical context. These experiments can serve in high school and undergraduate teaching, since they can be related directly to textbook knowledge of classical optics. Our work expands on an earlier discussion of fullerene diffraction in this journal in 2003,[28] explaining in more detail how to prepare and quantify transverse and longitudinal coherence of the molecular matter wave. To visualize the wave-particle duality, we use fluorescence imaging: Each molecule can be identified as a single particle on the detector, and a large number of molecules then lead to the emergence of a diffraction pattern, as shown before for single photons[29] and electrons.[30]

While diffraction of molecules and light share many fundamental features, we also see pronounced differences resulting from the particles' mass and electronic structure. Molecules fall visibly in the gravitational field, and they interact with the grating walls because of van der Waals forces. These forces are studied by rotating the grating relative to the molecular beam, which change with the average distance between the molecules and the slit wall. The role of the internal molecular structure opens numerous interesting questions, which are treated as problems and solutions for class work in the supplementary material.[31]

II. THEORY

A. Fraunhofer diffraction

Like many textbooks, we discuss diffraction through a thin mask in the far-field approximation, that is, in the Fraunhofer regime. In this regime, the curvature of the wavefronts can be neglected, and the diffracted intensity pattern is described by the Fourier transform of the transmission function of the diffracting mask (see the supplementary material[31]). Assuming an incident plane wave, the far-field assumption is valid when $L_2 \gg w^2/\lambda_{\mathrm{dB}}$, where L_2 is the distance between the mask and the detector, w is the width of the coherently illuminated mask, and λ_{dB} is the de Broglie wavelength (see Fig. 1). For $w = 300$ nm and

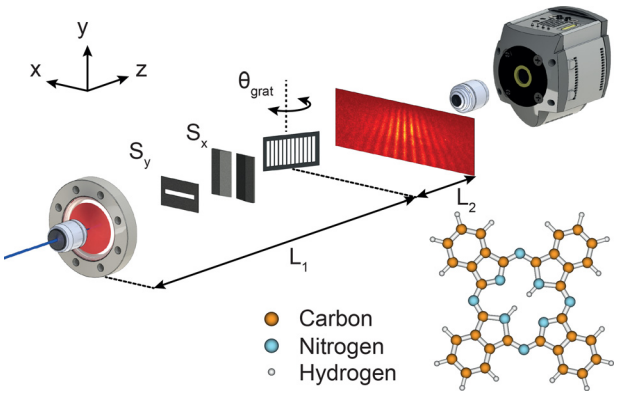

Fig. 1. Laser-evaporation of molecules leads to a beam, which is collimated along x and y. After 1.55 m of free flight, the matter wave is diffracted at a nanomechanical grating, which can be rotated by θ_{grat}. The resulting pattern is collected 0.59 m further downstream on a quartz plate and visualized via laser-induced fluorescence microscopy. We use the organic fluorophore phthalocyanine.

$\lambda_{\text{dB}} \simeq 3 \times 10^{-12}$ m, the transition region is <50 mm and, thus, considerably smaller than $L_2 = 590$ mm in our experiments. However, even when this requirement is not met, the far-field may still be a reasonable approximation (see the supplementary material[31]).

The non-relativistic de Broglie wavelength $\lambda_{\text{dB}} = h/mv$ depends on the particle's mass m and velocity v with Planck's constant h. If we neglect all internal properties, the intensity distribution I at an angle θ depends on the grating period d, the slit width s, and the number N of coherently illuminated slits

$$I(\theta) \propto \underbrace{\left(\frac{\sin\beta}{\beta}\right)^2}_{\text{single slit}} \underbrace{\left(\frac{\sin N\alpha}{\sin\alpha}\right)^2}_{\text{multiple slit}}, \tag{1}$$

with $\alpha = (\pi d/\lambda_{\text{dB}})\sin\theta$ and $\beta = (\pi s/\lambda_{\text{dB}})\sin\theta$. The first term in Eq. (1) describes diffraction through a single slit while the second term accounts for N-slit interference.

In quantum mechanics, we can additionally arrive at a similar prediction for the width of the central diffraction lobe based on Heisenberg's uncertainty relation. When a wave traverses a slit, its position is confined to the width s. This induces a transverse momentum uncertainty with a full width at half maximum (FWHM) of

$$\Delta p = 0.89\, h/s, \tag{2}$$

which evolves into a position uncertainty further downstream (see the supplementary material[31]). By measuring the beam's width, that is, its position uncertainty at the detector, we can, thus, extract Δp.[4,10] Within this envelope, a multipath interference pattern is formed when the wave is diffracted at two or more slits. Increasing the number N of illuminated slits sharpens the principal interference fringes and causes the occurrence of $N-2$ secondary maxima. The expected diffraction patterns behind a single, a double, and a triple slit are shown in Fig. 2.

B. Coherence

In order to observe multislit diffraction, the wavelets along different paths from the source to the detector need to have

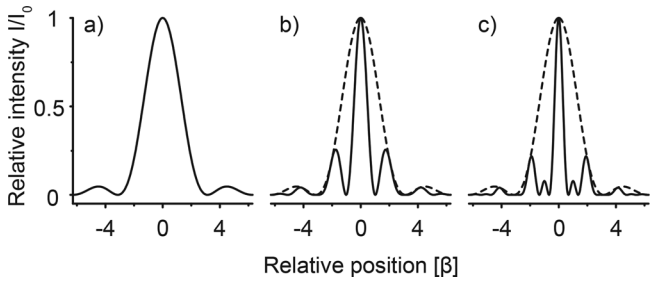

Fig. 2. Diffraction patterns through a single (a), a double (b), and a triple slit (c) according to Eq. (1). The envelope function is determined by the smallest diffraction element, i.e., the single slit, as indicated by the broken line for (b) and (c). The x-axis is given in multiples of $\beta = (\pi s/\lambda)\sin\theta$ and the opening fraction (slit width/period) is 0.65.

defined phase relations, i.e., they need to be coherent. Mathematically, coherence is defined as the normalized correlation function of the waves in space and time. There are several examples for coherent sources: lasers in optics or Bose–Einstein condensates in matter-wave science, where all photons or atoms are highly correlated over macroscopic distances in space and time. However, even thermal light and molecular beams can be prepared to be coherent.

It is often useful to distinguish between transverse and longitudinal coherence. As for laser radiation, they describe the distance along the propagation direction (longitudinal) and perpendicular to it (transverse) over which the phase of the matter wave is correlated.

Transverse coherence can be visualized as the uncertainty in the particle's transverse position, which makes it impossible to predict through which grating slit the particle will go. Since both the transverse coherence function and the diffraction pattern behind a single slit are described by a Fourier transform, they share the same functional form: $(\sin(x)/x)^2$.[32] If we define the transverse coherence width X_T by the distance between the first order minima of this coherence function, we find $X_T = 2L_1\lambda_{\text{dB}}/s$, which grows inversely proportional with the source width s (see the supplementary material[31]).

Longitudinal coherence is a measure of spectral purity of the beam and, thus, depends on the distribution of molecular velocities. If the distribution is too broad, the interference pattern vanishes, as soon as the constructive interference of one wavelength overlaps with the destructive interference of another one. This definition leads to the respective coherence length $X_L = \lambda^2/\Delta\lambda$. It differs by a factor of $1/2\pi$ from a definition based on propagating Gaussian wave packets.[33] However, it has proven surprisingly useful in real-world experiments, which are not necessarily well described by Gaussian wave packets (see the supplementary material[31]).

While the transverse coherence grows with the distance behind the source, this is not the case for the longitudinal coherence X_L, because the spectrum does not change in free flight. We can, however, increase X_L by spectral filtering, that is, by selecting molecular velocities.

III. EXPERIMENTAL SETUP

To record molecular diffraction patterns, we use the experimental setup sketched in Fig. 1.[34] A thin film of the molecule phthalocyanine (PcH_2, mass $m = 514.5$ u) is coated onto a window, which is mounted onto a vacuum chamber at a base pressure of $P < 1 \times 10^{-7}$ mbar. To launch the matter

wave, we focus a laser at $\lambda = 420\,\text{nm}$ with a 50× objective onto the film. This is where the first quantum effect comes into play: The position of the emitted molecules is defined by the spot size s_1 of the focused laser beam, which is twice the laser waist $s_1 = 2w_0 = (1.7 \pm 0.5)\ \mu\text{m}$. This localized evaporation can be seen as a position measurement. Approximating the evaporation spot as a rectangle, we can use Eq. (2) to estimate the associated transverse momentum uncertainty of $\Delta p \simeq 3.5 \times 10^{-28}$ kg m/s. When the molecules reach the grating after $L_1 = 1.55$ m, this has evolved into a position uncertainty. Heisenberg's principle, thus, helps us to prepare the transverse coherence required to illuminate several slits by the same molecular wave function. For PcH_2 moving at $v = 250$ m/s, the transverse coherence width amounts to $X_T \simeq 5.7\ \mu$m, i.e., 57 times the grating periods of 100 nm.

The grating was milled with a focused beam of gallium ions into an ultra-thin membrane of amorphous carbon with a thickness of $T = 21 \pm 2$ nm. A four-axis manipulator allows for 3D translations of the grating and a rotation around the y-axis. In our $(N = 1 - 3)$-slit gratings, the mean geometrical slit width amounts to $s_{\text{geo}} = 80 \pm 5$ nm, and the period is $d_{\text{geo}} = 100 \pm 5$ nm.[11] The bars between the slits have a cross section of $21 \times 20\,\text{nm}^2$, only an order of magnitude wider than the diameter of the diffracted molecule itself (1.5 nm). In the rotation experiments, we use a grating with $d_{\text{geo}} = 101 \pm 2$ nm and $s_{\text{geo}} = 61 \pm 1$ nm. The maximum width of the patterned area amounts to 5 μm and, thus, acts as a collimator in the x-direction. Additionally, the beam is loosely collimated by a piezo-controlled slit (S_x) to prevent transmission through membrane defects.

After passing the grating, the molecules are collected on a quartz plate $L_2 = 0.59$ m further downstream. To visualize the molecular density pattern, we excite PcH_2 with 60 mW of laser light at 661 nm focused onto a spot size of $400 \times 400\ \mu\text{m}^2$ and collect the laser-induced fluorescence with a 20× microscope objective. A band filter transmitting in the wavelength region from 700 to 725 nm is used to separate the fluorescence from the laser light, and the image is recorded with an electron multiplying (EM) CCD camera.

In the experiments, we use phthalocyanine (cf. Fig. 1) due to its high thermal stability and fluorescence quantum yield. This allows detection of single molecules with high contrast, which is required to visualize even weak signals.[34] Furthermore, PcH_2 is non-polar and, therefore, essentially unperturbed by residual charges in the mechanical masks.[35]

We use a thermal beam, containing a wide range of molecular velocities and, thus, de Broglie wavelengths. If all these velocities were to overlap at the detection screen, it would obscure many of the details present in the diffraction pattern. To prevent this, we restrict different velocities to different regions of the quartz plate. For that purpose, we use a horizontal delimiter S_y (see Fig. 3). In combination with the source, it defines the free-flight parabolas of the molecules in the presence of gravitational acceleration g. As the free-fall distance $H = g(L_1 + L_2)^2/(2v^2)$ depends on the molecular velocity v, slow molecules fall further than fast ones, and thus, they are separated at the position of the detector. In our few-slit diffraction experiment, the masks themselves serve as velocity selectors, for the case of the diffraction grating, an additional slit is introduced just before it.

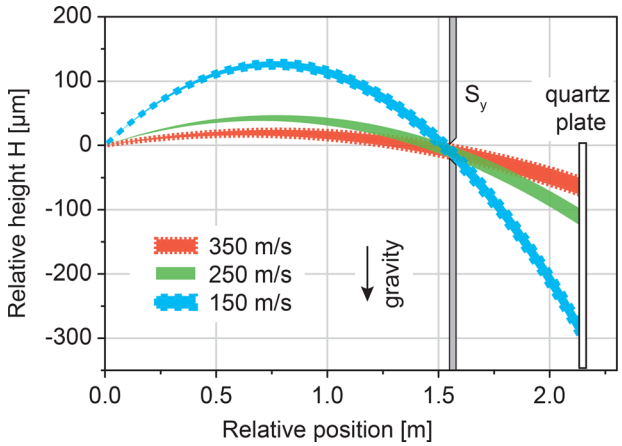

Fig. 3. The molecular beam spreads because of free-fall in the gravitational field. Molecules with a certain velocity pass the slit S_y to fall to a certain height on the detector. The free-fall distance and the separation of the molecular velocities grow quadratically with time. The thickness of S_y is not drawn to scale.

IV. DIFFRACTION THROUGH A FEW SLITS

A. Results

In Fig. 4, we show the results of molecular matter-wave diffraction at a single, a double, and a triple slit. The electron micrographs of the respective masks are shown in the upper trace, and the molecular diffraction patterns are shown in the middle trace. They span molecular velocities v between 140 and 430 m/s, corresponding to de Broglie

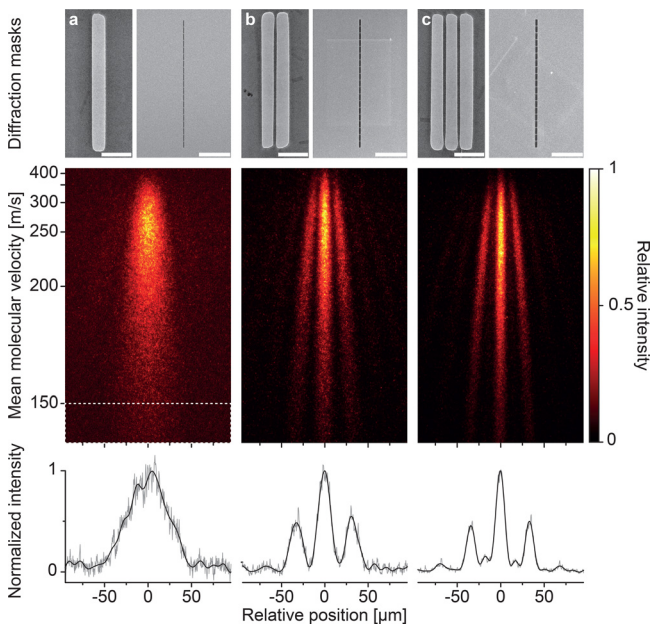

Fig. 4. Electron micrographs of a single (a), a double (b), and a triple slit (c) (Ref. 11). Each mask consists of 19 units of the original pattern placed above each other to increase the molecular flux. The slit width amounts to 80 ± 5 nm, and the period is 100 ± 5 nm. The scale bars correspond to 200 nm (left) and 5 μm (right), respectively. Sending molecular matter-waves through the masks results in diffraction patterns spanning the range from 140 to 430 m/s. The lower trace shows the vertical sum over the velocity band from 140 to 150 m/s, indicated by the broken line in the signal of the single-slit pattern. The summed traces are overlaid with a low pass filter with a spatial cut-off frequency of $1/12.5\ \mu$m.

wavelengths λ_{dB} between 5.5 and 1.8 pm. Each bright dot corresponds to a single molecule that scatters thousands of fluorescence photons during detection. At first glance, we observe a qualitative difference between the single-slit pattern and the other two: Diffraction at a single slit leads to a structureless, broad signal while the double- and triple-slit patterns exhibit a sub-structure. This is what we expect based on Eq. (1) and Fig. 2.

To illustrate the level of detail in the patterns, we vertically sum over the velocity band between 140 and 150 m/s as shown in the lower trace of Fig. 4. Here, all patterns share the same envelope resulting from single-slit diffraction. The triple slit pattern also reveals the expected secondary maximum in between the principal diffraction orders. Furthermore, the width of the zeroth diffraction order decreases with increasing N from 15.6 ± 0.1 μm for the double slit to 12.0 ± 0.1 μm for the triple slit.

It is often stated in textbooks that the wavelength has to be comparable to the grating period to observe interference. However, in the current experiments λ_{dB} is five orders of magnitude smaller than d, and still we observe high-contrast interference. To achieve this, we have to fulfill three conditions.

First, the transverse coherence has to be large enough to engulf all slits that shall contribute to multislit interference. As discussed before, X_T covers dozens of grating periods and, thus, exceeds the minimum requirement by far.

Second, the collimation angle has to be smaller than the diffraction angle $\theta = \lambda_{dB}/d$ to prevent the diffraction orders from overlapping. In our experiment, the width of the source ($s_1 = 1.7$ μm) and the grating ($w = 280$ nm for the triple slit) at a distance of $L_1 = 1.55$ m define a collimation angle of $\theta = (w + s_1)/L_1 = 1.3$ μrad. This is well below the diffraction angle of 31 μrad for PcH_2 moving at 250 m/s.

Finally, the resolution of the detector has to be sufficient to resolve the pattern. This is achieved using fluorescence microscopy: Each pixel in Fig. 4 images $400 \times 400\,\text{nm}^2$ on the fluorescence screen.[34] Curve fitting allows to determine the barycenter of the fluorescence curve with 10 nm accuracy and hence can easily resolve features on the μm-scale, as observed here.

B. Differences between light and matter waves

The patterns in Fig. 4 display many features also expected for light: the quantitative separation of the principal diffraction peaks, the emergence of the intermediate peaks for $N = 3$, and the narrowing of the principal diffraction orders with increasing N. However, there are also some major differences. The most outstanding feature is that the diffraction orders are not parallel but bent. Our source emits a distribution of molecular velocities, which is reflected in the spread of de Broglie wavelengths λ_{dB}. As the molecules follow free-flight parabolas in the gravitational field, all diffraction orders except the zeroth should be curved, as can be seen in Fig. 4.

The narrowing of the diffraction orders with increasing N is limited in our experiments. In the model of Eq. (1), the diffraction orders get sharper as long as N increases. In the experiments, however, the width of the diffraction orders has a lower bound defined by the transverse collimation angle, i.e., deviations from the assumption of an incident plane wave.

Also the envelope function hints at differences in the diffraction mechanism. From the micrographs, we extract a geometrical slit width $s_{geo} = 80 \pm 5$ nm. According to Eq. (2), this should lead to a diffraction envelope with a FWHM of 35 ± 2 μm at the detector for $v = 145$ m/s. However, we observe a width of 53 ± 1 μm, corresponding to an effective slit width s_{eff} of 53 ± 1 nm. The reason for this reduction is the van der Waals, or more generally, the Casimir–Polder interaction.

V. VAN DER WAALS INTERACTIONS

Casimir–Polder interactions result from fluctuations in the electron density of nearby objects.[36] As the maximum distance between molecule and the nearest grating bar is 40 nm during transmission, we are in the short range limit, known as the van der Waals interactions. Here, the induced dipole moments interact with their mirror images in the material. While the attractive potential scales with $1/x^6$ between two isolated particles, we have to integrate over the half-sphere of the grating, resulting in a potential, which scales with $1/x^3$.[37,38] Approximating the grating thickness T as infinite, the potential V_{pot} between the molecules and the grating can be written in the form $V_{pot}(x) = -C_3/x^3$. The factor C_3 includes the frequency-dependent polarizability of the particle and the dielectric function of the material grating, i.e., the response of both interaction partners to oscillating electric fields. This leads to a position-dependent phase ϕ, which is imprinted onto the molecular matter wave in each slit

$$\phi \simeq \exp\left(-\frac{i}{\hbar v}\int_0^T \frac{C_3}{(s/2-x)^3} + \frac{C_3}{(s/2+x)^3}\,dz\right). \tag{3}$$

The potential strongly depends on the distance $s/2 \pm x$ from the molecule to the grating walls, and we have to consider the influence of both walls in the slit, leading to a double-sided potential. The expression in Eq. (3) is justified for gratings, whose thickness is about 10^4 times the size of the diffracted particles.[39] For ultra-thin gratings, however, the molecule can actually be thicker than the grating itself.[40] Thus, the approach to the grating and the departure from it also have to be considered.[41]

To fully describe the interaction, we would have to characterize the molecule, the grating, and the interaction between them to a high level.[41,42] Such an analysis is very demanding: Each molecule consisting of n atoms has $3n - 6$ vibrations and many (often up to 500) rotational levels excited. Flexible molecules can adopt a number of different conformations, which may interconvert within picoseconds. Furthermore, the polarizability is often not isotropic, even for rigid molecules such as PcH_2. In consequence, the force depends on the orientation of the molecule during the transit through the grating. Moreover, charges implanted in the grating material may lead to an attractive force several times stronger than expected.[41]

Here, we resort to a phenomenological analysis: Close to the grating walls, the phase shift becomes so large that small position changes cause large phase fluctuations and the interference terms are averaged out. In a few nanometer distance, the molecule may even be adsorbed by the grating.[43] Hence, we divide the slit into two regions: In the center ϕ is small and multislit diffraction is possible. Close to the grating walls, however, the molecule cannot contribute to the

diffraction pattern any more. In this picture, the influence of the van der Waals interactions reduces the slit width from s_{geo} to an effective slit width s_{eff}.[39]

There are several options to modify the van der Waals interactions. First, altering the grating material changes the coefficient C_3, which determines the phase shift. Second, one can minimize the grating's thickness T—ultimately to just a single layer of atoms. This has recently been demonstrated using patterned single-layer graphene, which was stable enough to withstand the impact of fast molecules, and to yield high contrast molecule diffraction patterns.[40] Finally, we can change the molecule-grating distance and interaction length by rotating the grating.

VI. DIFFRACTION THROUGH A ROTATED GRATING

Rotating the grating modifies not only the effective grating period d_{eff} and slit width s_{eff} but also the interaction time and distance between the molecule and the grating walls. The molecules get close only to the edges of the grating, as shown in Fig. 5. This effect has been used to characterize nanomechanical gratings,[44,45] and the ensuing reduction in slit width was key to study weakly bound clusters.[46] In these experiments, the maximum angle of 42° was limited by the membrane thickness.[45] Here we use an ultra-thin grating with a thickness of $T = 21 \pm 2$ nm and a large opening fraction to achieve rotation angles up to 60°. This reduces the effective period by a factor of $\cos(60°) = 0.5$.

A. Results

The diffraction patterns recorded at $\theta_{grat} = 0°$, 40°, and 60° are shown in Fig. 6. They span molecular velocities v from 500 to 110 m/s, corresponding to de Broglie wavelengths λ_{dB} between 1.6 and 7.1 pm. For $\theta_{grat} = 0°$, the pattern is dominated by the zeroth and both first diffraction orders. Rotating the grating broadens the envelope function and shifts the position of the diffraction orders. For $\theta_{grat} = 40°$, the effective grating period $d_{eff} = d_{geo}\cos(\theta_{grat})$ is reduced to 77 nm, resulting in larger diffraction angles. Due to the grating thickness, the slit width is reduced from $s_{geo} = 61$ nm to $s_{eff} = 32$ nm. This confinement of the matter wave in the effective slit widens the single-slit envelope and leads to a stronger population of higher diffraction orders. In consequence, diffraction up to the $\pm 6th$ orders can be observed. At 60°, the effective period d_{eff} is half of the geometrical one, and the slit width is reduced by a factor of 5. At this angle, the diffraction envelope is about five times wider than under normal incidence.

We show typical traces for $v \sim 290$ m/s in the right column of Fig. 6. To assess s_{eff}, we fit a Gaussian to the maxima of the diffraction orders and convert its FWHM to the corresponding slit width utilizing Eq. (2). The width of the signal increases from 39 ± 1 (0°) to 184 ± 2 μm (60°), corresponding to a decrease in s_{eff} from 36 ± 1 to 8 ± 1 nm. Comparing the effective slit widths to the geometrical one (Table I)

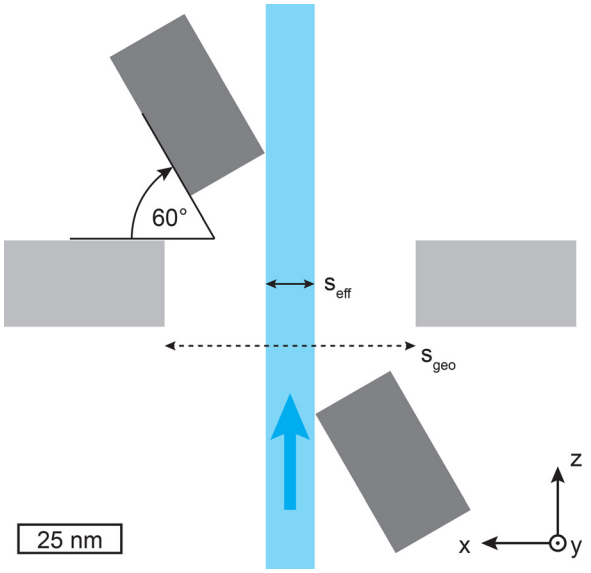

Fig. 5. Rotating the grating (light gray) by 60° (dark gray) reduces the projection of the geometrical slit width s_{geo} onto the molecular beam to s_{eff} (blue area). The molecules propagate in the direction of the blue arrow.

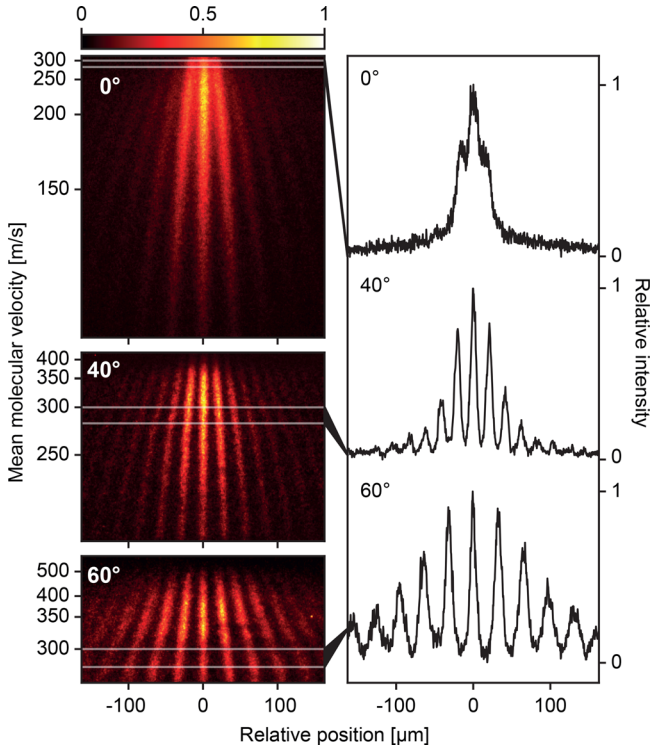

Fig. 6. Diffraction patterns for PcH_2 diffracted at the grating rotated by 0° (top), 40° (middle), and 60° (bottom). Rotating the grating reduces d_{eff} and s_{eff} and, thus, increases the separation of the peaks and widens the single-slit envelope. The traces in the right column show the vertical sum over the velocity band from 280 to 300 m/s. To determine s_{eff} the maxima of the peaks are fitted with a Gaussian. The FWHM of the Gaussian envelope amounts to 39 ± 1 μm (0°), 69 ± 1 μm (40°), and 184 ± 2 μm (60°). Each velocity axis has been scaled individually for best legibility.

Table I. Comparison of the geometry parameter for a mean velocity of 290 m/s. The difference Δ between the geometrical slit width s_{geo} and the effective one s_{eff} decreases considerably when rotating the grating from 0° to 60°.

	0°	40°	60°
s_{geo} (nm)	61 ± 1	32 ± 2	12 ± 2
FWHM (μm)	39 ± 1	69 ± 1	184 ± 2
s_{eff} (nm)	36 ± 1	20 ± 1	8 ± 1
$\Delta(s_{geo} - s_{eff})$ (nm)	25 ± 2	12 ± 3	4 ± 3

shows that the difference between them decreases with larger rotation angle: While the difference amounts to 25 ± 2 nm at perpendicular angle of incidence, it is reduced to only 4 ± 3 nm at 60°. However, such values have to be treated with care. Prior experiments have shown that the width of the envelope may be smaller than expected for slit widths of a few nanometer.[45] In consequence, s_{eff} extracted for 60° represents an upper bound.

VII. SUMMARY AND OUTLOOK

We have demonstrated molecular diffraction at a single-, double-, and triple slit as well as a rotated nanomechanical grating. Within the framework of the de Broglie hypothesis, the patterns agree astonishingly well with predictions from general wave optics, as used for light. However, we also observe pronounced differences, associated with the molecular mass and complex internal dynamics: Molecules fall visibly in the gravitational field and they are attracted by nearby walls. In the experiments presented here, the de Broglie wavelength ranges between 2 and 6 pm. Even though it is smaller than each molecule by about three orders of magnitude, we can see diffraction and a high-contrast interference pattern: Grating diffraction, thus, translates a relative path length difference of a few picometers into peak separations on the order of dozens of micrometers. This is a magnification by more than 10^6. In this respect, our experiments resemble small-angle X-ray scattering, aimed to reveal long range order in bio-systems. We have shown how this magnification can be utilized to visualize the force due to the van der Waals interaction, which is here on the atto-Newton level. It is interesting to see that matter-wave-based quantum technologies—using full multigrating interferometers—have started to generate impact in force and acceleration sensing applications.[47–49]

Matter-wave diffraction requires delicate setups, making it challenging for students to gain hands-on experience. A good alternative are online simulators, which provide a detailed lab environment and offer the possibility to perform realistic experiments life in class.[50,51]

The similarities and differences in the diffraction of matter and light are a good starting point to introduce matter-wave diffraction in introductory classes on quantum physics. To facilitate this, we include in the supplementary material[31] a number of problems and solutions related to our present experiments.

ACKNOWLEDGMENTS

The authors thank Thomas Juffmann and Joseph Cotter for work on that experiment as well as Yigal Lilach for writing the masks. This project has received funding from the Austrian Science Fund (FWF) within Project No. P-30176.

[a]Electronic mail: Christian.Brand@dlr.de

[1]G. Möllenstedt and C. Jönsson, "Elektronen-Mehrfachinterferenzen an regelmäßig hergestellten Feinspalten," Z. Phys. **155**, 472–474 (1959).
[2]C. Jönsson, "Elektroneninterferenzen an mehreren künstlich hergestellten Feinspalten," Z. Phys. **161**, 454–474 (1961).
[3]R. Bach, D. Pope, S.-H. Liou, and H. Batelaan, "Controlled double-slit electron diffraction," New J. Phys. **15**, 033018 (2013).
[4]C. G. Shull, "Single-slit diffraction of neutrons," Phys. Rev. **179**, 752–754 (1969).
[5]A. Zeilinger, R. Gähler, C. G. Shull, W. Treimer, and W. Mampe, "Single- and double-slit diffraction of neutrons," Rev. Mod. Phys. **60**, 1067–1073 (1988).
[6]O. Carnal and J. Mlynek, "Young's double-slit experiment with atoms: A simple atom interferometer," Phys. Rev. Lett. **66**, 2689–2692 (1991).
[7]F. Shimizu, K. Shimizu, and H. Takuma, "Double-slit interference with ultracold metastable neon atoms," Phys. Rev. A **46**, R17–R20 (1992).
[8]Y. Shin, M. Saba, T. A. Pasquini, W. Ketterle, D. E. Pritchard, and A. E. Leanhardt, "Atom interferometry with Bose-Einstein condensates in a double-well potential," Phys. Rev. Lett. **92**, 050405 (2004).
[9]P. Szriftgiser, D. Guéry-Odelin, M. Arndt, and J. Dalibard, "Atomic wave diffraction and interference using temporal slits," Phys. Rev. Lett. **77**, 4–7 (1996).
[10]O. Nairz, M. Arndt, and A. Zeilinger, "Experimental verification of the Heisenberg uncertainty principle for fullerene molecules," Phys. Rev. A **65**, 032109 (2002).
[11]J. P. Cotter, C. Brand, C. Knobloch, Y. Lilach, O. Cheshnovsky, and M. Arndt, "In search of multipath interference using large molecules," Sci. Adv. **3**, e1607478 (2017).
[12]D. W. Keith, M. L. Schattenburg, H. I. Smith, and D. E. Pritchard, "Diffraction of atoms by a transmission grating," Phys. Rev. Lett. **61**, 1580–1583 (1988).
[13]D. M. Tennant, J. E. Bjorkholm, M. L. O'Malley, M. M. Becker, J. A. Gregus, and R. W. Epworth, "Free standing silicon microstructures for soft x-ray masks and cold atom focusing," J. Vac. Sci. Technol. B **8**, 1975–1979 (1990).
[14]O. Carnal, M. Sigel, T. Sleator, H. Takuma, and J. Mlynek, "Imaging and focusing of atoms by a Fresnel zone plate," Phys. Rev. Lett. **67**, 3231–3234 (1991).
[15]J. Fujita, M. Morinaga, T. Kishimoto, M. Yasuda, S. Matsui, and F. Shimizu, "Manipulation of an atomic beam by a computer-generated hologram," Nature **380**, 691–694 (1996).
[16]R. B. Doak, R. E. Grisenti, S. Rehbein, G. Schmahl, J. P. Toennies, and C. Wöll, "Towards realization of an atomic de Broglie microscope: Helium atom focusing using Fresnel zone plates," Phys. Rev. Lett. **83**, 4229–4232 (1999).
[17]W. Schöllkopf and J. P. Toennies, "Nondestructive mass selection of small van der Waals clusters," Science **266**, 1345–1348 (1994).
[18]R. E. Grisenti, W. Schöllkopf, J. P. Toennies, G. C. Hegerfeldt, T. Köhler, and M. Stoll, "Determination of the bond length and binding energy of the helium dimer by diffraction from a transmission grating," Phys. Rev. Lett. **85**, 2284–2287 (2000).
[19]A. R. Barnea, O. Cheshnovsky, and U. Even, "Matter-wave diffraction approaching limits predicted by Feynman path integrals for multipath interference," Phys. Rev. A **97**, 023601 (2018).
[20]A. D. Cronin and B. McMorran, "Electron interferometry with nanogratings," Phys. Rev. A **74**, 061602 (2006).
[21]G. Gronniger, B. Barwick, and H. Batelaan, "A three-grating electron interferometer," New J. Phys. **8**, 224 (2006).
[22]G. van der Zouw, M. Weber, J. Felber, R. Gähler, P. Geltenbort, and A. Zeilinger, "Aharonov-Bohm and gravity experiments with the very-cold-neutron interferometer," Nucl. Instrum. Methods Phys. Res., Sect. A **440**, 568–574 (2000).
[23]D. W. Keith, C. R. Ekstrom, Q. A. Turchette, and D. E. Pritchard, "An interferometer for atoms," Phys. Rev. Lett. **66**, 2693–2696 (1991).
[24]B. Brezger, L. Hackermüller, S. Uttenthaler, J. Petschinka, M. Arndt, and A. Zeilinger, "Matter-wave interferometer for large molecules," Phys. Rev. Lett. **88**, 100404 (2002).
[25]S. Gerlich, L. Hackermüller, K. Hornberger, A. Stibor, H. Ulbricht, M. Gring, F. Goldfarb, T. Savas, M. Muri, M. Mayor, and M. Arndt, "A Kapitza–Dirac–Talbot–Lau interferometer for highly polarizable molecules," Nat. Phys. **3**, 711–715 (2007).
[26]Y. Y. Fein, P. Geyer, P. Zwick, F. Kiałka, S. Pedalino, M. Mayor, S. Gerlich, and M. Arndt, "Quantum superposition of molecules beyond 25 kDa," Nat. Phys. **15**, 1242–1245 (2019).
[27]S. Sala, A. Ariga, A. Ereditato, R. Ferragut, M. Giammarchi, M. Leone, C. Pistillo, and P. Scampoli, "First demonstration of antimatter wave interferometry," Sci. Adv. **5**, eaav7610 (2019).
[28]O. Nairz, M. Arndt, and A. Zeilinger, "Quantum interference experiments with large molecules," Am. J. Phys. **71**, 319–325 (2003).
[29]T. L. Dimitrova and A. Weis, "The wave-particle duality of light: A demonstration experiment," Am. J. Phys. **76**, 137–142 (2008).
[30]A. Tonomura, J. Endo, T. Matsuda, T. Kawasaki, and H. Ezawa, "Demonstration of single-electron buildup of an interference pattern," Am. J. Phys. **57**, 117–120 (1989).

[31]See supplementary material at https://www.scitation.org/doi/suppl/10.1119/5.0058805 for more information about the transition between the near- and far-field, molecular coherence, beam properties, as well as problems and solutions.
[32]M. Born and E. Wolf, *Principles of Optics*, 7th ed. (Cambridge U. P., Cambridge, 1997).
[33]C. S. Adams, M. Sigel, and J. Mlynek, "Atom optics," Phys. Rep. **240**, 143–210 (1994).
[34]T. Juffmann, A. Milic, M. Müllneritsch, P. Asenbaum, A. Tsukernik, J. Tüxen, M. Mayor, O. Cheshnovsky, and M. Arndt, "Real-time single-molecule imaging of quantum interference," Nat. Nanotechnol. **7**, 297–300 (2012).
[35]C. Knobloch, B. A. Stickler, C. Brand, M. Sclafani, Y. Lilach, T. Juffmann, O. Cheshnovsky, K. Hornberger, and M. Arndt, "On the role of the electric dipole moment in the diffraction of biomolecules at nanomechanical gratings," Fortschr. Phys. **65**, 1600025 (2017).
[36]H. B. G. Casimir and D. Polder, "The influence of retardation on the London-van der Waals forces," Phys. Rev. **73**, 360–372 (1948).
[37]M. E. Mullins, L. P. Michaels, V. Menon, B. Locke, and M. B. Ranade, "Effect of geometry on particle adhesion," Aerosol Sci. Technol. **17**, 105–118 (1992).
[38]J. E. Lennard-Jones, "Process of adsorption and diffusion on solid surfaces," Trans. Faraday Soc. **28**, 333–359 (1932).
[39]R. E. Grisenti, W. Schöllkopf, J. P. Toennies, G. C. Hegerfeldt, and T. Köhler, "Determination of atom-surface van der Waals potentials from transmission-grating diffraction intensities," Phys. Rev. Lett. **83**, 1755–1758 (1999).
[40]C. Brand, M. Sclafani, C. Knobloch, Y. Lilach, T. Juffmann, J. Kotakoski, C. Mangler, A. Winter, A. Turchanin, J. Meyer, O. Cheshnovsky, and M. Arndt, "An atomically thin matter-wave beamsplitter," Nat. Nanotechnol. **10**, 845–848 (2015).
[41]C. Brand, J. Fiedler, T. Juffmann, M. Sclafani, C. Knobloch, S. Scheel, Y. Lilach, O. Cheshnovsky, and M. Arndt, "A Green's function approach to modeling molecular diffraction in the limit of ultra-thin gratings," Ann. Phys. (Berlin, Ger.) **527**, 580–591 (2015).
[42]J. Fiedler and S. Scheel, "Casimir-Polder potentials on extended molecules," Ann. Phys. (Berlin, Ger.) **527**, 570–579 (2015).
[43]T. Juffmann, S. Nimmrichter, M. Arndt, H. Gleiter, and K. Hornberger, "New prospects for de Broglie interferometry," Found. Phys. **42**, 98–110 (2012).
[44]A. D. Cronin and J. D. Perreault, "Phasor analysis of atom diffraction from a rotated material grating," Phys. Rev. A **70**, 043607 (2004).
[45]R. E. Grisenti, W. Schöllkopf, J. P. Toennies, J. R. Manson, T. A. Savas, and H. I. Smith, "He-atom diffraction from nanostructure transmission gratings: The role of imperfections," Phys. Rev. A **61**, 033608 (2000).
[46]R. Brühl, A. Kalinin, O. Kornilov, J. P. Toennies, G. C. Hegerfeldt, and M. Stoll, "Matter wave diffraction from an inclined transmission grating: Searching for the elusive ^{4}He trimer Efimov state," Phys. Rev. Lett. **95**, 063002 (2005).
[47]M. Arndt, "De Broglie's meter stick: Making measurements with matter waves," Phys. Today **67**(5), 30–36 (2014).
[48]G. Tino and M. Kasevich, *Atom Interferometry: Proceedings of the International School of Physics "Enrico Fermi"* (IOS, Varenna, 2014), Vol. 188.
[49]W. P. Schleich, K. S. Ranade, C. Anton, M. Arndt, M. Aspelmeyer, M. Bayer, G. Berg, T. Calarco, H. Fuchs, E. Giacobino, M. Grassl, P. Hänggi, W. M. Heckl, I.-V. Hertel, S. Huelga, F. Jelezko, B. Keimer, J. P. Kotthaus, G. Leuchs, N. Lütkenhaus, U. Maurer, T. Pfau, M. B. Plenio, E. M. Rasel, O. Renn, C. Silberhorn, J. Schiedmayer, D. Schmitt-Landsiedel, K. Schönhammer, A. Ustinov, P. Walther, H. Weinfurter, E. Welzl, R. Wiesendanger, S. Wolf, A. Zeilinger, and P. Zoller, "Quantum technology: From research to application," Appl. Phys. B **122**, 130 (2016).
[50]See <https://interactive.quantumnano.at/letsgo/> for "Quantum Interactive" (2015).
[51]M. Tomandl, T. Mieling, C. M. Losert-Valiente Kroon, M. Hopf, and M. Arndt, "Simulated interactive research experiments as educational tools for advanced science," Sci. Rep. **5**, 14108 (2015).